OFFICE OF NAVAL RESEARCH

Contract No. N00014-91-J-1409

Technical Report No. 118

The Emergence of Atomic-Level Structural Information for Ordered Metal-Solution Interfaces: Some Recent Contributions from In-Situ Infrared Spectroscopy and Scanning Tunneling Microscopy

by

X. Gao, S.-C. Chang, X. Jiang, A. Hamelin,

and M.J. Weaver

Prepared for Publication

in the

Journal of Vacuum Science & Technology A

Purdue University

Department of Chemistry

West Lafayette, Indiana 47907

February 1992

SECURITY CLASSIFICATION OF THIS PAGE

REPORT DOCUMENTATION PAGE

Form Approved
OMB No 0704-0188

1a REPORT SECURITY CLASSIFICATION Unclassified	1b RESTRICTIVE MARKINGS
2a SECURITY CLASSIFICATION AUTHORITY	3 DISTRIBUTION/AVAILABILITY OF REPORT Approved for public release and sale; its distribution is unlimited.
2b DECLASSIFICATION/DOWNGRADING SCHEDULE	
4 PERFORMING ORGANIZATION REPORT NUMBER(S) Technical Report No. 118	5 MONITORING ORGANIZATION REPORT NUMBER(S)
6a NAME OF PERFORMING ORGANIZATION Purdue University Department of Chemistry 6b OFFICE SYMBOL (If applicable)	7a NAME OF MONITORING ORGANIZATION Division of Sponsored Programs Purdue Research Foundation
6c ADDRESS (City, State, and ZIP Code) Purdue University Department of Chemistry West Lafayette, IN 47907	7b ADDRESS (City, State, and ZIP Code) Purdue University West Lafayette, IN 47907
8a NAME OF FUNDING/SPONSORING ORGANIZATION Office of Naval Research 8b OFFICE SYMBOL (If applicable)	9 PROCUREMENT INSTRUMENT IDENTIFICATION NUMBER Contract No. N00014-91-J-1409
8c ADDRESS (City, State, and ZIP Code) 800 N. Quincy Street Arlington, VA 22217	10 SOURCE OF FUNDING NUMBERS PROGRAM ELEMENT NO / PROJECT NO / TASK NO / WORK UNIT ACCESSION NO

11 TITLE (Include Security Classification)
The Emergence of Atomic-Level Structural Information for Ordered Metal-Solution Interfaces: Some Recent Contributions from In-Situ Infrared Spectroscopy and Scanning Tunneling Microscopy.

12 PERSONAL AUTHOR(S)
Xiaoping Gao, Si-Chung Chang, Xudong Jiang, Antoinette Hamelin, and Michael J. Weaver

13a TYPE OF REPORT	13b TIME COVERED	14 DATE OF REPORT (Year, Month, Day)	15 PAGE COUNT
Technical	FROM _____ TO _____	February 28, 1992	

16 SUPPLEMENTARY NOTATION

17 COSATI CODES			18 SUBJECT TERMS (Continue on reverse if necessary and identify by block number)
FIELD	GROUP	SUB-GROUP	infrared reflection-absorption spectroscopy, scanning tunneling microscopy, metal-ultrahigh vacuum surfaces, potential-dependent properties of saturated CO adlayers.

19 ABSTRACT (Continue on reverse if necessary and identify by block number)

The utilization of infrared reflection-absorption spectroscopy (IRAS) and scanning tunneling microscopy (STM) to extract atomic-resolution information for ordered metal-solution interfaces in a related (and relatable) fashion to metal-ultrahigh vacuum (uhv) surfaces is illustrated by means of some recent results from our laboratory. Two specific topics are addressed. The first involves the potential-dependent properties of saturated CO adlayers on low-index platinum and rhodium electrodes in aqueous and nonaqueous media. The central role of the surface potential in controlling the CO adlayer structure is discussed on the basis of in-situ IRAS data, especially in comparison with the properties of corresponding metal-uhv interfaces. The application of in-situ atomic-resolution STM in tandem with IRAS for elucidating real-space adsorbate structures is noted for saturated CO adlayers on Rh(111) and Rh(110) electrodes. The second topic concerns the application of in-situ STM to probe potential-induced

20 DISTRIBUTION/AVAILABILITY OF ABSTRACT ☐ UNCLASSIFIED/UNLIMITED ☐ SAME AS RPT ☐ DTIC USERS	21 ABSTRACT SECURITY CLASSIFICATION
22a NAME OF RESPONSIBLE INDIVIDUAL	22b TELEPHONE (Include Area Code) / 22c OFFICE SYMBOL

DD Form 1473, JUN 86 Previous editions are obsolete. SECURITY CLASSIFICATION OF THIS PAGE

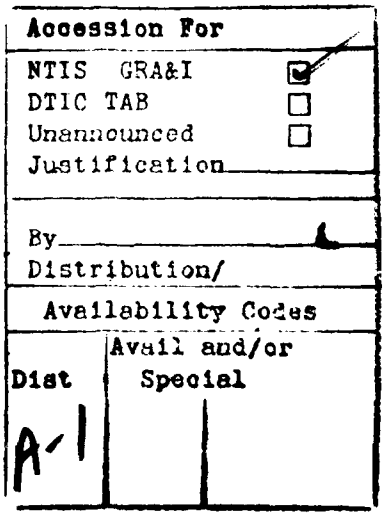

(19. cont.)

reconstruction at gold-aqueous interfaces. All three low-index gold surfaces are seen to undergo reconstruction at potentials corresponding to small (ca 10-15 $\mu C\ cm^{-2}$) negative electrode charges. The subtle surface relaxation observed for Au(111) is essentially identical to that observed recently by atomic-resolution STM in uhv (ref. 45). The (5 x 27) and (1 x n) (n = 2,3) symmetries observed for reconstructed Au(100) and (110) electrodes, respectively, are compatible with the structures deduced for the uhv systems by diffraction methods, although the STM data afford greater real-space detail.

ABSTRACT

The utilization of infrared reflection-absorption spectroscopy (IRAS) and scanning tunneling microscopy (STM) to extract atomic-resolution information for ordered metal-solution interfaces in a related (and relatable) fashion to metal-ultrahigh vacuum (uhv) surfaces is illustrated by means of some recent results from our laboratory. Two specific topics are addressed. The first involves the potential-dependent properties of saturated CO adlayers on low-index platinum and rhodium electrodes in aqueous and nonaqueous media. The central role of the surface potential in controlling the CO adlayer structure is discussed on the basis of in-situ IRAS data, especially in comparison with the properties of corresponding metal-uhv interfaces. The application of in-situ atomic-resolution STM in tandem with IRAS for elucidating real-space adsorbate structures is noted for saturated CO adlayers on Rh(111) and Rh(110) electrodes. The second topic concerns the application of in-situ STM to probe potential-induced reconstruction at gold-aqueous interfaces. All three low-index gold surfaces are seen to undergo reconstruction at potentials corresponding to small (ca 10-15 $\mu C\ cm^{-2}$) negative electrode charges. The subtle surface relaxation observed for Au(111) is essentially identical to that observed recently by atomic-resolution STM in uhv (ref. 45). The (5 x 27) and (1 x n) (n = 2,3) symmetries observed for reconstructed Au(100) and (110) electrodes, respectively, are compatible with the structures deduced for the uhv systems by diffraction methods, although the STM data afford greater real-space detail.

INTRODUCTION

As for metal surfaces in ultrahigh vacuum (uhv) environments, a major goal in electrochemical surface science is to elucidate the structural properties of metal-solution interfaces and to relate them to the kinetic, especially catalytic, processes that can occur there. Several factors, however, have conspired these two fundamentally related areas to develop in distinctly different directions. Most obviously, the early emergence of uhv technology itself along with reliable means of both preparing and characterizing ordered monocrystalline metal surfaces in uhv has led to a major and continuing emphasis being placed on the atomic-level structural characterization of such systems. In physical electrochemistry, particular attention was drawn instead to the mercury-aqueous interface. This emphasis resulted not only from the high degree of cleanliness and reproducibility that can be achieved, but also from the detailed thermodynamic analyses that can be undertaken at such liquid-liquid interfaces, yielding accurate surface compositional parameters. As a consequence of the ease by which rate measurements can be made in electrochemical systems by means of faradaic current flow, much attention has also been given to elucidating reaction kinetics at such surfaces and relating them to the interfacial structure.

Given the major advances evident in the structural characterization of metal-uhv surfaces, electrochemists have nevertheless long been motivated by a desire to "bridge the (pressure) gap" between electrochemical and uhv systems, in an experimental as well as conceptual fashion. A prominent experimental avenue, developed originally by Hubbard et al.[1], involves emersing monocrystalline electrodes from solution under potential control and transferring them into uhv. Such "ex-situ" procedures have the major virtue of enabling the full range of uhv-based techniques to be harnessed for electrode surface characterization.

On the other hand, the approach is limited by the inevitable removal of volatile surface components and other structural changes that can attend solution-uhv electrode transfer. Another insightful approach involves dosing appropriate molecular components of electrochemical interfaces, especially solutes, solvents, and ionizable species, onto the surface held at sufficiently low temperatures in uhv. This "uhv electrochemical modeling" procedure, pioneered by Sass and coworkers[2], enables the mutual influence of the various components of the so-called "electrochemical double layer" on adsorbate structure to be examined in sequential fashion. In particular, the effect of varying the interfacial ("electrode") potential can be mimicked by monitoring the changes in work function caused by dosing dipolar and ionizable species.

Despite the power of these ex-situ approaches, it is apparent that the development of molecular- (and atomic-) level techniques applicable to "in-situ" electrochemical systems, i.e., with the metal surface in solution under potential control, is of great importance. The relative paucity of the latter applications in the past has been due to the inevitable difficulties in accessing the surface by means of probe photons, electrons, etc., in the presence of a macroscopic solution phase. An additional impediment has been the lack of reliable procedures for preparing ordered metal surfaces for inspection in an ambient laboratory environment. In the last ten years or so, however, the use of various flame-annealing and related procedures has been shown to yield well-ordered surfaces for several metals of electrochemical importance, including platinum[3,4], rhodium[4b], gold, and silver.[5] In turn, the emergence of such straightforward methods of preparing ordered metal surfaces in electrochemical environments is giving new impetus to the usage as well as development of in-situ methods for examining interfacial atomic and molecular structure.

In this conference paper, we summarize and assess some recent activities

being pursued in our laboratory along these lines using two such in-situ approaches: infrared reflection-absorption spectroscopy (IRAS) and scanning tunneling microscopy (STM). While quite different in character, both these techniques share the virtue of being applicable in a similar fashion to both metal-uhv and metal-solution interfaces. As a consequence, they offer so-far unusual, and even unique, opportunities to explore atomic- and molecular-level phenomena at electrochemical surfaces in the same fashion as the detailed structural information which is familiar for related metal-uhv systems. The links thus forged between these two major variants of metal interfaces should therefore be of significance to surface science as a whole.

We restrict attention here to a brief description of selected applications of IRAS and STM, both separately and in tandem, to the elucidation of surface structure at ordered platinum, rhodium, and gold electrodes in aqueous and nonaqueous media. Experimental and other salient details can be found in the references cited. Two specific issues are addressed here. The first involves the potential-dependent properties of saturated CO adlayers on low-index platinum and rhodium, and the second concerns potential-dependent reconstruction on ordered gold. Both these types of examples emphasize the central role played by the applied surface potential in controlling the interfacial structural properties. Besides illustrating how IRAS and STM can provide structural information for metal-solution as well as metal-uhv surfaces at the atomic level, they also offer the prospect that examining the former systems by this means can prove to be of mutual benefit to both research arenas.

Potential-Dependent Infrared Spectra for CO Adlayers: Comparisons between Electrochemical and UHV Systems

Carbon monoxide constitutes an adsorbate of archetypical importance in electrochemical as well as uhv surface science. Its significance to the former

class of systems arises in part from the common role of CO as an adsorbed poison towards the catalytic electrooxidation of a variety of organic molecules on platinum and other transition-metal electrodes.[6] From a fundamental perspective, adsorbed CO has some unique attributes as a structure-sensitive model adsorbate for intercomparing the properties of ordered metal surfaces in electrochemical and uhv environments. Most importantly, the frequency of the C-O infrared stretching vibration (ν_{co}) is extremely sensitive to the surface coordination geometry as well as the local chemical and electrostatic environment; as a consequence, IRAS provides an excellent means of exploring the molecular-level adlayer properties.

Following the development of IRAS for examining adsorbates at metal-uhv interfaces[7], the last decade has seen a substantial growth in the application of this technique to in-situ electrochemical surfaces.[8] The complications arising from bulk-phase solvent and other interferences can be minimized and even eliminated by the use of thin-layer electrochemical tactics combined with potential-difference spectral techniques.[8] In our laboratory, we have utilized in-situ IRAS extensively to explore the structural and kinetic properties of CO adlayers on low-index platinum and rhodium electrodes.[9-17] A recent detailed overview article describing several aspects of this work is available.[9] A basic experimental tactic utilized in these studies is the systematic acquisition of infrared spectra as a function of adsorbate coverage, θ_{co}, and electrode potential, E. The former can shed light on the roles of adlayer domain formation and solvent and/or hydrogen coadsorption on the adlayer structure; the latter measurements provide direct assessments of the variable influence of the electrostatic double layer.[9]

We will restrict attention here to ordered metal surfaces containing saturated CO adlayers, formed by dosing with solutions containing near-saturated

CO concentrations. In this way, we can minimize (or even eliminate) the influence of solvent coadsorption, and examine the effect of varying the potential across the adlayer on the spectral properties. Figure 1 shows a typical sequence of infrared spectra for a saturated CO adlayer on Pt(111) in acetonitrile, taken from ref. 16a. The E values indicated are the electrode potentials (versus aqueous saturated calomel electrode, SCE) to which each spectrum refers. Most notably, the ν_{co} frequencies of both the higher and lower frequency bands, diagnostic of terminal and bridging CO coordination, respectively, upshift progressively as E is increased. These ν_{co} – E dependencies have been ascribed either to potential-induced alterations in the metal-CO bonding, or to a first-order Stark effect arising from variations in electrostatic field across the CO adlayer.[18] [In all likelihood, both of these descriptions are incomplete by themselves. Self-consistent treatments, which take into account both surface bonding and field-induced effects, have been described recently in principle.[19]] In addition, Fig. 1 shows that the bridging band undergoes a sharp ca 50 cm^{-1} frequency upshift at ca 0 V vs SCE (Fig. 1). This discontinuity, together with a concomitant alteration of both the terminal and bridging ν_{co} – E slopes at this point, are indicative of a potential-induced adlayer structural change at 0 V vs SCE.[16a]

It is of central interest to relate these potential-dependent spectral properties to the behavior of the corresponding uhv system. A perusal of the electrochemical infrared spectra at the highest potentials, ca 1.0 V vs SCE, indicate a similarity to those obtained for saturated (θ_{co} ~ 0.6) CO adlayers on Pt(111) in uhv[20], in that the intensities of the terminal relative to the bridging band are comparable, and both bands exhibit similar ν_{co} frequencies (within ca 10 cm^{-1}) in the two environments.[16a]

These similarities, together with related results for other metal/CO

adlayer systems, prompt consideration of the potential-dependent nature of such electrochemical surfaces in comparison with metal-uhv systems.[9] The key difference between these two types of metal interfaces is that the metal-solution potential drop, ϕ_s^M, can be varied continuously by altering the electrode potential E, whereas the potential drop across metal-vacuum interfaces, ϕ_v^M, is usually fixed for a given metal and adsorbate composition. Physically, this difference arises from the presence of free charges at electrochemical interfaces, where the excess (or deficiency) of electronic charge accumulated at the metal surface (by virtue of its connection to an external power source) is countered by an equal and opposite ionic charge present, usually as solvated ions at the so-called "outer Helmholtz plane" (oHp), on the solution side of the interface. (The metal-solution interface can therefore be conceived of as a parallel-plate capacitor.)

At the so-called potential of zero charge, E_{pzc}, this free-charge contribution to ϕ_s^M disappears, at least in the absence of ionic chemisorption, as would be anticipated in the presence of saturated CO adlayers. We have obtained approximate estimates of E_{pzc} for Pt(111)/CO and other low-index Pt/CO and Rh/CO interfaces in nonaqueous solvents by examining ν_{co} - E dependencies in electrolytes containing organic cations having different radii.[16] [Note that cations, rather than anions, will accumulate in excess at the oHp in these systems since the electrode potentials accessed lie largely below (i.e., negative of) the E_{pzc}.] The different double-layer thicknesses, and hence distinct interfacial potential profiles, thus generated yield dissimilar ν_{co} - E slopes that should intersect at E_{pzc}.[16] This procedure yields relatively high E_{pzc} values; for Pt(111)/CO, for example, $E_{pzc} \simeq 1.0$ V vs SCE (equivalent to 1.25 V vs the normal hydrogen electrode, NHE). The ν_{co} - E plots are found to be insensitive to the solvent,[13] suggesting that solvent dipole orientation

contributes little to the surface potential drop, as might be expected in the presence of a saturated CO adlayer.

On this basis, then, one can surmise that at $E = E_{pzc}$ the metal-solution potential drop ϕ_s^M present at, say, Pt(111)/CO electrochemical interfaces will be similar to ϕ_v^M for the corresponding Pt(111)/CO surface in uhv. From the above information, the ν_{co} frequencies for Pt(111)/CO in the former environment are seen to converge to those in the latter system when $E \approx E_{pzc}$, inferring that a major factor influencing the CO adlayer structure is indeed the average surface potential drop in both cases.

The relation between measured potentials for metal-solution and metal-uhv systems has engendered considerable discussion.[21,22] For the latter interfaces, work-function (Φ_v) measurements provide a direct route to evaluating ϕ_v^M, since $\Phi_v = e\phi_v^M$. The assessment of the corresponding metal-solution potential drop, ϕ_s^M, from electrode potential measurements is less straightforward since the latter are actually potential *differences with respect to a reference electrode*. The required link with metal-vacuum systems can be made by assessing the so-called "absolute" potential of the reference electrode used, $E_k(ref)$,[21] equal to the potential of the reference electrode metal versus vacuum. If $E_k(ref)$ is known, then we can extract ϕ_s^M from the measured electrode potential by using[9]

$$\phi_s^M = E + E_k(ref) - \chi_s \qquad (1)$$

where χ_s is the surface potential of the solution-vacuum interface.[21] (This quantity is commonly estimated to be small, so that $|\chi_s| \lesssim 0.1 - 0.2$ V.)

There is some controversy regarding the appropriate values of $E_k(ref)$, usually considered for the normal hydrogen electrode (NHE). While thermodynamic arguments have led to a value of about 4.45 V for $E_k(ref)$ of the NHE,[21] higher estimates, 4.7–4.8 V, have been obtained from work-function measurements for

electrodes transferred into uhv[22] and by other means.[23] Using an average value, $E_k(ref) = 4.6 \pm 0.2$ V, and given that E_{pzc} for the Pt(111)/CO electrochemical interface (in acetonitrile) is about 1.25 V vs NHE (vide supra), if χ_s is neglected we deduce from Eq(1) that the metal-solution potential drop at E_{pzc} is $\phi_s^M \simeq 5.9$ V. Interestingly, the latter value is essentially equal to the potential drop at the Pt(111)/CO–vacuum interface, ϕ_v^M, as extracted from work-function measurements.[11b] This identity deduced between ϕ_s^M for the *uncharged* electrochemical system and ϕ_v^M for the corresponding (necessarily uncharged) metal-uhv interface further supports the major role played by the surface potential drop in controlling the adlayer properties.

It is appropriate to comment further on the potential-induced changes in the CO adlayer properties observed at transition-metal electrochemical interfaces in comparison with the metal-uhv systems. Under most circumstances, the electrode potential ranges accessible in electrochemical environments lie well (~ 1 to 2V) below E_{pzc}, i.e., correspond to negative electrode charges. This is especially the case in aqueous media, where adsorbed CO electrooxidation to form CO_2 typically occurs at low potentials. Nevertheless, most IRAS studies of this type in our laboratory as well as elsewhere have utilized aqueous, and especially acidic aqueous, media. There are several reasons for this choice, including the use of surface pretreatment procedures that utilize aqueous solutions, and the occurrence of voltammetric features in such media that have proved to be diagnostic of the surface order.[3,4]

A notable feature of the CO adlayer structures on low-index platinum and especially rhodium electrodes is the sensitivity of the CO binding geometries to the electrode potential.[9,10] Decreasing the potential (so to increase the negative charge density) tends to favor increasingly bridging versus atop CO coordination.[9,10] The effect can be understood qualitatively in terms of the

increased degree of $d\pi - 2\pi^*$ metal–ligand back bonding that occurs as the metal charge becomes more negative.[9,10,17] In addition, the CO coordination geometry is sensitive to both the nature of the metal surface and its crystallographic orientation.[9,10] These latter effects by themselves are well known from studies of the corresponding metal–uhv interfaces. Significantly, different surface-dependent CO binding geometries, however, can be obtained in electrochemical environments due to the additional influence of the applied potential.[9,10]

Theoretical understanding of these trends has so far been pursued largely on a qualitative level. The molecular orbital (ASED–MO[26]) method of Anderson, involving potential-induced shifts in the surface valence-band energy,[8a] has been used with some success to describe CO site occupancies on Pt and Pd surfaces,[27] and to account for the marked differences in potential-dependent CO binding geometries observed on Rh(111) versus Rh(100).[17] In addition, the ASED–MO model can account semiquantitatively for the observed[9,10,15] propensity for atop versus bridging coordination on (111) planes for Pt-group metals in the sequence Ir > Pt > Rh > Pd.[28] While the ASED–MO method does therefore appear to provide a useful semi-empirical means of describing potential-dependent surface bonding, as noted above it ignores the influence of electrostatic field on the adsorbate, presuming tacitly that the surface potential drop falls entirely *between* the metal and the adsorbate molecule; it also does not consider explicitly the surface charge density. A more self-consistent picture of potential-dependent surface binding, taking these combined factors into account,[19] will hopefully be forthcoming.

STM and IRAS as Combined Probes of Adlayer Structure: CO on Rh(111) and Rh(110) Electrodes

While IRAS can yield detailed insight into the coordination geometry of CO and other suitable adsorbates, it lacks the spatial information required to

deduce real-space adlayer structures. In uhv environments, such information is commonly provided by low-energy electron diffraction (LEED). In a number of cases, the required spatial structural arrangement of the adlayer with respect to the underlying substrate have been deduced from the LEED adlayer symmetry in combination with site occupancies as obtained from vibrational spectra.[29] Such tactics are inapplicable to in-situ electrochemical interfaces, where LEED usually cannot be employed. However, the recent emergence of STM as a *truly* atomic-resolution structural probe applicable to metal-solution,[30,31] as well as with other metal (and semiconductor), interfaces is beginning to change this situation. Indeed, in suitable cases atomic-resolution STM offers a detailed assessment of the real-space adlayer structure, rather than merely an assignment of the unit-cell symmetry as is commonly extracted from LEED measurements. (The deduction of the real-space adlayer arrangement within the unit cell requires dynamical LEED analyses, the execution of which is usually not unambiguous.)

A difficulty with STM, however, is that at the present stage of technique development the interpretation of atomic-resolution images is often not clearcut. Apart from the need for near-optimal tunneling conditions so to obtain the desired spatial resolution, the surface electronic properties that determine the observed images are incompletely understood. For these reasons, together with the need to match the adlayer structure with that of the underlying substrate (i.e., determine adsorbate surface binding sites), it is desirable to couple STM with an independent in-situ structural probe, such as IRAS.

We have chosen for initial study in this regard saturated CO adlayers on low-index rhodium-aqueous interfaces. Pertinent results are summarized here for Rh(111) and (110); original STM data are shown for the latter surface since they are unavailable elsewhere. As already mentioned, significantly potential-dependent CO structures are often deduced from IRAS, arising from the increased

propensity for bridging versus terminal coordination as the electrode potential is decreased. For Rh(111) in aqueous 0.1 M $NaClO_4$, in particular, a relatively sharp, yet reversible, structural transition from primarily terminal to bridging CO coordination is observed as the potential is lowered below ca −0.1 to −0.2 V vs SCE.[10a]

The extraction of detailed adlayer structures from a comparison between the corresponding potential-dependent IRAS and STM data for Rh(111)/CO is outlined in ref. 32. Briefly, at potentials above where adsorbed CO electrooxidation proceeds (ca 0.3 V), well-defined STM images of the Rh(111) substrate are obtained, consisting specifically of image "spots" (tunneling maxima) spaced in a hexagonal array 2.7Å apart. At lower potentials, where the close-packed CO adlayers are present, markedly different STM images were obtained that reflect the structure of the adlayer rather than the underlying substrate.

Significantly, two distinct images are obtained over the same potential regions where the two CO adlayer structures, as deduced by IRAS, are present. At potentials above ca −0.1 V vs SCE, a structure having (2 x 2)−3CO symmetry is discerned. The CO coverage thus deduced, $\theta_{CO} = 0.75$, is in agreement with the value determined from voltammetry and infrared spectrophotometry. Of the three distinguishable STM spots within the (2 x 2) unit cell, two are noticeably "brighter" (i.e., induce greater tunneling current). The corresponding IRAS data show the presence of two-thirds of the adsorbate ($\theta_{CO} = 0.5$) present in atop (or near-atop) sites, with one-third ($\theta_{CO} = 0.25$) in a bridging coordination, (as deduced by ν_{CO} bands at 2025–2045 cm^{-1} and 1800–1820 cm^{-1}, respectively). On this basis, then, the brighter and weaker STM spots are attributed to tunneling via atop and bridging CO's, respectively; this conclusion is also consistent with the intuitive prediction of greater tunneling current (at constant tip-surface separation) via the atop adsorbate. A very similar (2 x 2) structure for the

Rh(111)/CO (θ_{CO} = 0.75) surface in uhv was deduced earlier on the basis of dynamical LEED measurements.[33] The occurrence of such similar adlayer structures at the electrochemical interface at higher potentials with the corresponding uhv system is in harmony with the important role of surface potential in determining adlayer structure, outlined above.

At potentials below −0.2 V, markedly different STM images, having (3 x √3 rect)−4CO symmetry (θ_{CO} = 0.67), are obtained. Matching these results again with the corresponding IRAS data, only a single CO in the unit cell is identified as atop, two of the three remaining CO's being present in asymmetric bridging sites (appearing as a prominent ν_{CO} band at 1885–1900 cm^{-1}). Both the high- and low-potential adlayer structures appear to represent a compromise between the energetic preferences for CO binding, favoring atop and bridging CO coordination, respectively, and the surface stereochemical constraints necessary to reach the observed high packing densities (cf ref. 20b).

In contrast to Rh(111), saturated CO adlayers on Rh(110) display no sharp potential-dependent changes in binding geometry as deduced from IRAS. Thus over the potential range −0.25 to 0.25 V vs SCE in 0.1 M $HClO_4$, both atop and bridging ν_{CO} features are observed (at 2020–2040 cm^{-1} and 1890 to 1910 cm^{-1}, respectively) with comparable integrated intensities, even though the latter binding mode is favored increasingly towards lower potentials.[10a] Comparison with the corresponding Pt(110) system illustrates the anticipated greater propensity for bridging versus atop CO coordination on rhodium; while the saturated CO coverage is essentially unity on both surfaces, Pt(110) displays almost entirely terminal coordination.[10a,12c]

A typical atomic-resolution STM image for Rh(110) in CO-saturated 0.1 M $HClO_4$ (at −0.2 V vs SCE) is displayed in Fig. 2. (See the figure caption along with ref. 32 for STM procedural details. The Rh(110) crystal, 9mm diameter and

2mm thick, was pretreated by a flame-annealing/iodine coating procedure as in ref. 13a (cf ref. 4).) The image is seen to consist of strings of individually resolved spots (i.e., regions of higher tunneling current in a direction ca 20° to the x axis. These rows correspond closely to the [1$\bar{1}$0] direction as discerned from X-ray back diffraction. Comparable images were obtained over the potential range −0.25 to 0.1 V vs SCE. Several properties of the STM images (as seen in Fig. 2) enable the CO adlayer symmetry to be deduced. First, the distances between spots along the [1$\bar{1}$0] direction, 3.5Å, and across these rows in the [001] direction, 2.75Å, both differ from those expected (and observed) for the (1 x 1) Rh(110) surface,[34] 2.7 and 3.8Å, respectively.[35] [The x and y distances evaluated by the STM piezoelectric drivers are calibrated by examining substrate images for well-defined surfaces, such as Au(111) and Rh(111), and are reliable to ca ±10%.] Second, instead of the spots in adjacent rows being lined up in the [001] direction, as for the substrate atoms or for a (1 x 1) commensurate adlayer (θ_{CO} = 1.0), they are seen to form parallel lines running at ca 75° to the [1$\bar{1}$0] direction (Fig. 2).

These two pieces of information both indicate that an adlayer (rather than a substrate) image is obtained for the Rh(110)/CO (θ_{CO} = 1) surface, which is not commensurate in simple fashion with the metal lattice. Nevertheless, a definite symmetry of the adlayer with respect to the substrate can be confirmed from the mild yet discernable intensity pattern in the STM spots, whereby every third spot along the [1$\bar{1}$0] rows tends to be more intense. Assuming, as before, that such spots are associated with CO bound to symmetric atop sites leads to the suggested *"ball-model" adlayer structure* shown in Fig. 3. (The fine-shaded, and open circles in Fig. 3 depict the CO adsorbate, and Rh surface atoms, respectively.) The (4 x 3)-12CO structure depicted matches well with the STM images (see the corresponding unit cell superimposed on Fig. 2), and has the correct CO coverage

(θ_{CO} = 1.0).

Careful inspection of Fig. 3 reveals that besides the single symmetric atop CO (located on the corners of the unit cell as drawn), most of the remaining CO's are situated in asymmetric atop or bridging sites. This structure might appear to be in disagreement with the corresponding IRAS data which, as noted above, consists of only two *discrete* ν_{CO} bands diagnostic of terminal and bridging coordination geometries.[10a] While the infrared spectra certainly cannot confirm the STM-deduced adlayer structure, the two data sets are, however, not inconsistent. Thus the terminal ν_{CO} frequency is expected to be insensitive to displacement away from symmetrical atop sites, and distributions of nearby CO's in similar, yet distinct, sites can appear as single relatively narrow ν_{CO} bands as a result of intensity transfer effects.[20] At least qualitatively, then, the appearance of a pair of broad, relatively asymmetric, ν_{CO} bands in the infrared spectra, nominally associated with atop and bridging configuration,[10a] is in reasonable harmony with the real-space adlayer structure as deduced from STM.

As for the Rh(111) surface, the structure of saturated CO adlayers on Rh(110) appears to result from adsorbate packing considerations intertwined with site-specific binding energies. A similarly complex (2 x 4) structure for saturated CO on Rh(100) in aqueous 0.1 M $HClO_4$ has also been deduced from STM,[36] reflecting a combination of atop and bridge-bound adsorbate as seen by IRAS.[10a,13b] It would be of great interest to pursue STM measurements for these and other CO adlayer systems in related uhv environments. It is nonetheless appropriate to point out an important (perhaps obvious) limitation of such STM measurements: the extraction of such real-space atomic structures requires that the adlayer is extremely immobile. Adsorbate motion of only several angstroms on the long ($\gtrsim 10^{-1}$s) timescale required to obtain at least a portion of the STM x-y scan should seriously "blur" the resulting image. The compressed CO adlayers

are presumably sufficiently immobile to satisfy this requirement.

Potential-Dependent Surface Reconstruction as Probed by Atomic-Resolution STM

This article has so far concentrated on one specific, albeit important, topic: the structural properties of CO adlayers on transition-metal electrodes. As already noted, STM also offers considerable promise for elucidating the atomic structure of ordered metal surfaces in the absence of chemisorbed adlayers.[30] While low-index rhodium surfaces usually display simple bulk-terminated [i.e., (1 x 1)] surface structures even in the absence of chemisorption, many other metal surfaces are known to reconstruct to form markedly different atomic rearrangements.[37] An interesting example is gold, especially so since emersion of low-index gold electrodes from solution into uhv, followed by LEED and related characterization, have indicated the presence of potential-dependent surface reconstruction, triggered at lower electrode potentials.[38] We have recently utilized in-situ STM to explore in detail the electrode potential-induced reconstruction of both ordered low- and higher-index gold surfaces in aqueous solution.[39-42] The primary findings, particularly as they relate to the behavior of the corresponding gold-uhv interfaces, are summarized briefly here.

The Au(111)-uhv surface is unique among fcc metals in undergoing a subtle, yet significant, reconstruction as deduced originally by diffraction techniques,[43] and latterly in remarkable detail by atomic-resolution STM.[44,45] The ($\sqrt{3}$ x 22) reconstruction features a periodic alteration from fcc to hcp stacking, yielding parallel pairs of mild corrugations along one of the $[11\bar{2}]$ directions, i.e., at an angle midway between a pair of intersecting close-packed atomic rows. Intriguingly, an essentially identical reconstruction pattern is observed by STM at the Au(111)-aqueous 0.1 M $HClO_4$ interface at potentials below ca -0.1 V vs SCE, i.e., at small negative electrode charge densities (ca -10 to -15 μC cm^{-2}).[40] Moreover, most of the longer-range superstructures occurring in the uhv

system are also observed in the in-situ electrochemical environment. An interesting difference, however, is that an essentially unreconstructed Au(111) surface is obtained at E_{pzc} (0.25 V vs SCE),[40] even though the Au(111)–uhv surface is also necessarily uncharged (vide supra). This difference may well be due to the influence of the interfacial water, or conceivably to adsorbed perchlorate anions.

Both Au(100) and (110) in aqueous 0.1 M $HClO_4$ are also largely unreconstructed at E_{pzc}, yet undergo marked reconstruction at somewhat (0.2 – 0.3 V) lower potentials.[39,41] Figure 4 shows a representative height-shaded STM image, viewed 30° off the surface normal, obtained for Au(100) at –0.3 V vs SCE (see ref. 39 for details). Evident are corrugated strings of atoms which form in a given ([0$\bar{1}$1] and [011]) direction along the previously square-planar (1 x 1) lattice. A buckled quasi-hexagonal arrangement is formed, featuring six atoms packed across each corrugation, replacing five atoms in the (1 x 1) structure.

In addition, large ordered domains exhibit a regular longer-range periodicity along the row direction, featuring undulations of the gold strings (see Fig. 4). These 14-atom periodic transitions (between structures I and II as described in ref. 39) yield a mild compression along the row direction, so that 28 atoms are present in place of 27 for the unreconstructed surface. The net (5 x 27) symmetry designation of the Au(100) reconstruction is compatible with earlier detailed diffraction analyses for clean Au(100) in uhv,[43,46] although the latter *reciprocal-space* techniques cannot diagnose such structures with confidence. [We will discuss the assignment of this structure in detail elsewhere.[42]] In keeping with the substantial (24%) increase in forming the (5 x 27) structure from the (1 x 1) square-planar lattice, the reconstruction dynamics are slow, requiring ca 10 mins. for completion at –0.3 to –0.4 V. The STM images also indicate that the additional gold atoms diffuse from terrace and

other domain edges.

Figure 5 is an illustrative height-shaded STM image, again viewed 30° off the surface normal, for Au(110) in 0.1 M $HClO_4$ at -0.3 V vs SCE. (See ref. 41 for details.) This image shows the characteristic feature of the Au(100) reconstruction: stacked sets of parallel ribbon segments, running along the [1$\bar{1}$0] crystallographic direction. Each ribbon consists of a trio of three parallel rows of gold atoms. The spacing between these ribbons is mostly (4.0 x n)Å, where n = 2 or 3, i.e., corresponding to (1 x 2) or (1 x 3) symmetries, respectively. The former symmetry corresponds to the "missing-row" reconstruction commonly proposed for clean Au(110) in uhv.[47] However, detailed examination of the (1 x 2) STM images indicates that some "surface relaxation" occurs, involving both the top and underlying gold atoms so to form a significant asymmetric structure involving pairing of second-layer atoms.[41]

The (1 x 3) regions, exemplified in the bottom left-hand segment of the image in Fig. 5, appear as separated ribbons overlaid on the underlying substrate. In this sense, the resulting structures can be viewed as forming "added-", rather than "missing-", row domains. The concerted motion of atoms required to form (or remove) such reconstructions appear to involve migration both across and along the rows. The small and rather irregular domain sizes observed typically on reconstructed Au(110) suggest that only short-range atomic motion is required. Consistent with this last feature is the observation that the potential-induced structural changes are surprisingly rapid as well as near-reversible, the reconstruction being lifted largely within ca 2s upon stepping the potential from -0.3 to 0 V vs SCE, and reappearing on the same timescale when the potential is returned to -0.3 V.[41]

As for Au(111), both Au(100) and (110) form stable (1 x 1) structures in the aqueous electrochemical environment at E_{pzc}, whereas the corresponding clean

surfaces in uhv are reconstructed. Nevertheless, the role of negative surface electronic charge density in triggering reconstruction is in harmony with some theoretical predictions for low-index noble metal surfaces.[48]

Most recently, we have examined potential-dependent structures of higher-index, especially stepped, gold surfaces, such as Au(210), (533), (311), and (221) in 0.1 M $HClO_4$. Perhaps surprisingly, these surfaces undergo only mild reconstruction, occurring again at negative electrode charges, that involves slight relaxation of the atoms forming (or adjacent to) the monoatomic steps. These results will be described in detail elsewhere[42]; they offer significant implications for the interpretation of surface crystallographic effects on electrocatalytic processes.[49]

While the foregoing is necessarily an incomplete summary, focussing only on recent results from our own laboratory, it is now evident that both IRAS and STM can provide molecular- and atomic-level structural information for ordered metal-solution interfaces at a level of detail (and understanding) which is on a par with the well-established applications of these techniques to metal-uhv systems. While experimental inquiries for electrochemical interfaces along these general lines have been pursued for some time by means of ex-situ emersion procedures,[1] the development of such in-situ techniques offers a significant new dimension in electrochemical surface characterization. Together, then, this expanding family of experimental methods should encourage an increasing commonality of understanding in electrochemical and ultrahigh vacuum surface science.

ACKNOWLEDGMENTS

This work is supported by the National Science Foundation and the Office of Naval Research.

REFERENCES

1. For example: A.T. Hubbard, Chem. Rev., 88, 633 (1988)

2. For example: J.K. Sass, K. Bange, ACS Symp. Ser., 378, 54 (1988)

3. (a) J. Clavilier, R. Faure, G. Guinet, R. Durand, J. Electroanal. Chem., 107, 205 (1980); (b) Also see: J. Clavilier, ACS Symp. Ser., 378, 202 (1988)

4. (a) D. Zurawski, L. Rice, M. Hourani, A. Wieckowski, J. Electroanal. Chem., 230, 221 (1987); (b) M. Hourani, A. Wieckowski, J. Electroanal. Chem., 227, 259 (1987)

5. A. Hamelin, in "Modern Aspects of Electrochemistry", B.E. Conway, R.E. White, J.O'M. Bockris, eds, Plenum, New York, Vol. 16, 1986, Chapter 1

6. For example: L.-W.H. Leung, M.J. Weaver, Langmuir, 6, 323 (1990)

7. For example: A.M. Bradshaw, E. Schweizer, in "Spectroscopy of Surfaces", Advances in Spectroscopy, Vol. 16, R.J.H. Clark, R.E. Hester, eds, Wiley, New York, 1988, p.413

8. (a) A. Bewick, S. Pons, in "Advances in Infrared and Raman Spectroscopy", Vol. 12, R.J.H. Clark, R.E. Hester, eds, Wiley, New York, 1985, Chapter 1; (b) P. Christensen, A. Hamnett, in "Comprehensive Chemical Kinetics", Vol. 29, R.G. Compton, A. Hamnett, eds, Elsevier, Amsterdam, 1989, Chapter 1

9. For an overview: S.-C. Chang, M.J. Weaver, J. Phys. Chem., 95, 5391 (1991)

10. (a) S.-C. Chang, M.J. Weaver, Surface Sci., 238, 142 (1990); (b) S.-C. Chang, J.D. Roth, Y. Ho, M.J. Weaver, J. Electron. Spect. Relat. Phenom., 54/55, 1185 (1990)

11. (a) L.-W.H. Leung, A. Wieckowski, M.J. Weaver, J. Phys. Chem., 92, 6985 (1988); (b) S.-C. Chang, L.-W.H. Leung, M.J. Weaver, J. Phys. Chem., 93, 5341 (1989)

12. (a) S.-C. Chang, M.J. Weaver, J. Chem. Phys., 92, 4582 (1990); (b) S.-C. Chang, M.J. Weaver, J. Phys. Chem., 94, 5095 (1990); (c) S.-C. Chang, M.J. Weaver, Surface Sci., 230, 222 (1990); (d) J.D. Roth, S.-C. Chang, M.J. Weaver, J. Electroanal. Chem., 288, 255 (1990); (e) S.-C. Chang, J.D. Roth, M.J. Weaver, Surface Sci., 244, 113 (1991)

13. (a) L.-W.H. Leung, S.-C. Chang, M.J. Weaver, J. Chem. Phys., 90, 7426 (1989); (b) S.-C. Chang, M.J. Weaver, J. Electroanal. Chem., 285, 263 (1990)

14. S.-C. Chang, M.J. Weaver, Surface Sci., 241, 11 (1991)

15. X. Jiang, S.-C. Chang, M.J. Weaver, J. Phys. Chem., 95, 7453 (1991)

16. (a) S.-C. Chang, X. Jiang, J.D. Roth, M.J. Weaver, J. Phys. Chem., 95, 5378 (1991); (b) X. Jiang, M.J. Weaver, in preparation

17. S.-C. Chang, A.B. Anderson, M.J. Weaver, J. Phys. Chem., in press

18. (a) A.B. Anderson, J. Electroanal. Chem., 280, 37 (1990); (b) D.K. Lambert, J. Chem. Phys., 89, 3847 (1988), and previous references cited therein

19. H.J. Kreuzer, in "Chemistry and Physics of Solid Surface VIII, Springer Series in Surface Sciences", Vol. 22, R. Vanselow, R. Howe, eds, Springer-Verlag, Berlin, 1990

20. For example: (a) E. Schweizer, B.N.J. Persson, M. Tüshaus, D. Hoge, A.M. Bradshaw, Surface Sci., 213, 49 (1989); (b) B.N.J. Persson, M. Tüshaus, A.M. Bradshaw, J. Chem. Phys., 92, 5034 (1990)

21. S. Trasatti, J. Electroanal. Chem., 150, 1 (1983)

22. For a brief overview: W.N. Hansen, G.J. Hansen, ACS Symp. Ser., 378, 166 (1988)

23. R. Kötz, H. Neff, K. Müller, J. Electroanal. Chem., 215, 331 (1986)

24. R. Gomer, G. Tryson, J. Chem. Phys., 66, 4413 (1977)

25. For example: J.E.B. Randles, Phys. Chem. Liquids, 7, 63 (1977)

26. ASED-MO - "atom superposition and electron delocalization molecular orbital" method[18a]

27. (a) A.B. Anderson, M.K. Awad, J. Am. Chem. Soc., 107, 7854 (1985); (b) S.P. Mehandru, A.B. Anderson, J. Phys. Chem., 93, 2044 (1989)

28. S.-C. Chang, A.B. Anderson, M.J. Weaver, unpublished results

29. (a) J.P. Biberian, M.A. Van Hove, Surface Science, 138, 361 (1984); (b) J.P. Biberian, M.A. Van Hove, Surface Science, 118, 443 (1982)

30. O.M. Magnussen, J. Hotlos, R.J. Nichols, D.M. Kolb, R.J. Behm, Phys. Rev. Lett., 64, 2929 (1990)

31. S.-L. Yau, C.M. Vitus, B.C. Schardt, J. Am. Chem. Soc., 112, 3677 (1990)

32. S.-L. Yau, X. Gao, S.-C. Chang, B.C. Schardt, M.J. Weaver, J. Am. Chem. Soc., 113, 6049 (1991)

33. M.A. Van Hove, R.J. Koestner, J.C. Frost, G.A. Somorjai, Surface Science, 129, 482 (1983)

34. Unlike Pt(110), even clean Rh(110) does not appear to undergo surface reconstruction.[35]

35. For example: (a) M. Bowker, Q. Guo, R. Joyner, Surface Science, 253, 33 (1991); (b) K. Lehnberger, W. Nichtl-Pecher, W. Oed, K. Heinz, K. Muller, Surface Science, 217, 511 (1989)

36. C. Vitus, Ph.D. thesis, Purdue University, 1991

37. For example: G.A. Somorjai, M.A. Van Hove, Prog. Surf. Science, 30, 201 (1989)

38. (a) M.S. Zei, G. Lehmpfuhl, D.M. Kolb, Surface Science, 221, 23 (1989); (b) D.M. Kolb, J. Schneider, Electrochim. Acta., 31, 929 (1986)

39. X. Gao, A. Hamelin, M.J. Weaver, Phys. Rev. Lett., 67, 618 (1991)

40. X. Gao, A. Hamelin, M.J. Weaver, J. Chem. Phys., 95, 6993 (1991)

41. X. Gao, A. Hamelin, M.J. Weaver, Phys. Rev. B., in press

42. X. Gao, A. Hamelin, M.J. Weaver, manuscripts in preparation

43. M.A. Van Hove, R.J. Koestner, P.C. Stair, J.P. Biberian, L. Kesmodel, I. Bartos, G. Somorjai, Surface Science, 103, 189 (1981)

44. C. Wöll, S. Chiang, R.J. Wilson, P.H. Lippel, Phys. Rev. B., 39, 7988 (1989)

45. J.V. Barth, H. Brune, G. Ertl, R.J. Behm, Phys. Rev. B., 42, 9307 (1990)

46. K.H. Rieder, T. Engel, R.H. Swendsen, M. Manninen, Surface Science, 127, 223 (1983)

47. For example: E. Vlieg, I.K. Robinson, K. Kern, Surface Scinece, 233, 248 (1990)

48. (a) K.-M. Ho, K.P. Bohnen, Phys. Rev. Lett., 59, 1833 (1987); (b) V. Heine, L.D. Marks, Surface Science, 165, 65 (1986)

49. Y. Ho, S.-C. Chang, A. Hamelin, M.J. Weaver, Langmuir, in press

FIGURE CAPTIONS

Fig. 1

Sequences of infrared absorbance spectra in the C–O stretching region for CO adlayer on Pt(111) in CO-saturated acetonitrile containing 0.15 M tetrabutylammonium perchlorate, obtained during 2 mV s^{-1} positive-going potential sweep from -1.6 V vs SCE. Each spectrum involved acquiring 100 interferometer scans (consuming ca 60s), subtracted from which was a similar set of scans obtained after complete CO electrooxidation, at ca 1.0 V. Potentials indicated alongside each spectrum are average values (vs SCE) during the spectral acquisition (see ref. 16a for further details).

Fig. 2

Mildly FT-filtered top-view STM image of (4 x 3)-12CO structure obtained for Rh(110) in CO-saturated aqueous 0.1 M $HClO_4$ at -0.2 V vs SCE. Rectangle shown refers to unit cell as depicted in Fig. 3. Image was obtained in "constant-height" mode. Tunneling conditions: bias voltage $V_b = 4$ mV, set-point current $i_t = 20$ nA.

Fig. 3

Proposed top-view ball model for (4 x 3)-12CO adlayer structure on Rh(110). The top-layer rhodium atoms are depicted as the larger circles, with smaller circles representing position of individual CO adsorbate molecules as deduced from STM image in Fig. 2 (see text for details).

Fig. 4

Height-shaded STM image for reconstructed Au(100) surface in aqueous 0.1 M $HClO_4$ at -0.4 V vs SCE. Image was obtained in "constant-current" mode. Tunneling conditions: $V_b = 10$ mV, $i_t = 20$ nA. (See ref. 39 for other details.)

Fig. 5

Height-shaded STM image of reconstructed Au(110) surface in aqueous 0.1 M $HClO_4$ at -0.3 V vs SCE, showing (1 x 2) and (1 x 3) regions. Image was obtained in "constant-current" mode. Tunneling conditions: $V_b = 5$ mV, $i_t = 25$ nA.

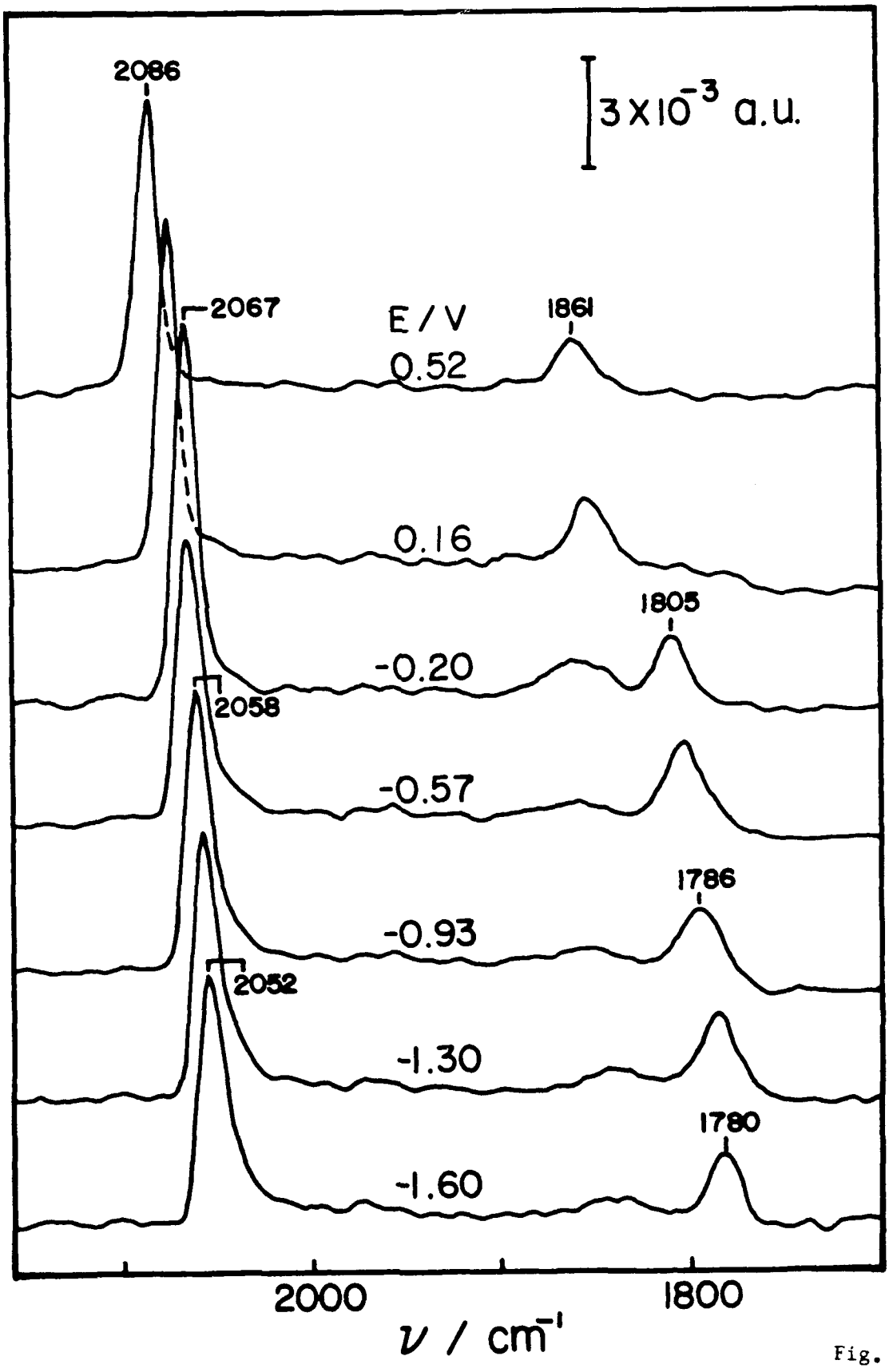
2086
3X10⁻³ a.u.
2067
E / V
1861
0.52
0.16
1805
-0.20
2058
-0.57
1786
-0.93
2052
-1.30
1780
-1.60
2000
1800
ν / cm⁻¹

Fig. 1

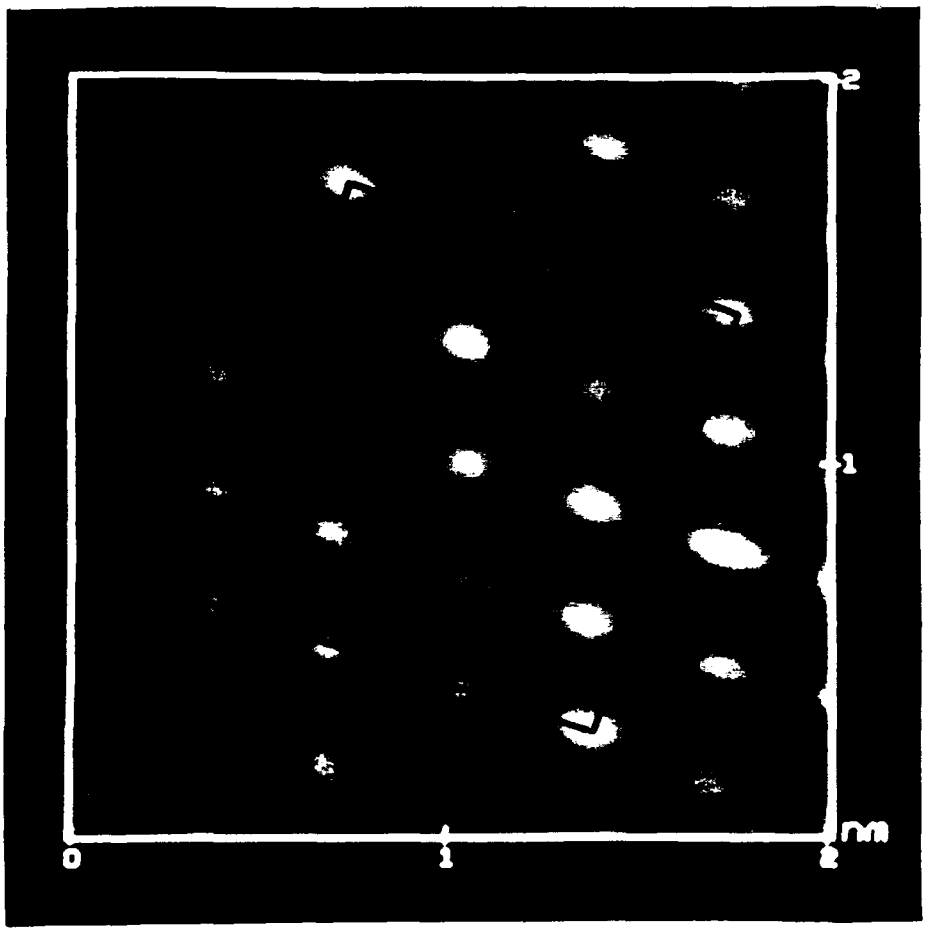

FIG 2

Rh(110)-CO, (4x3) Structure

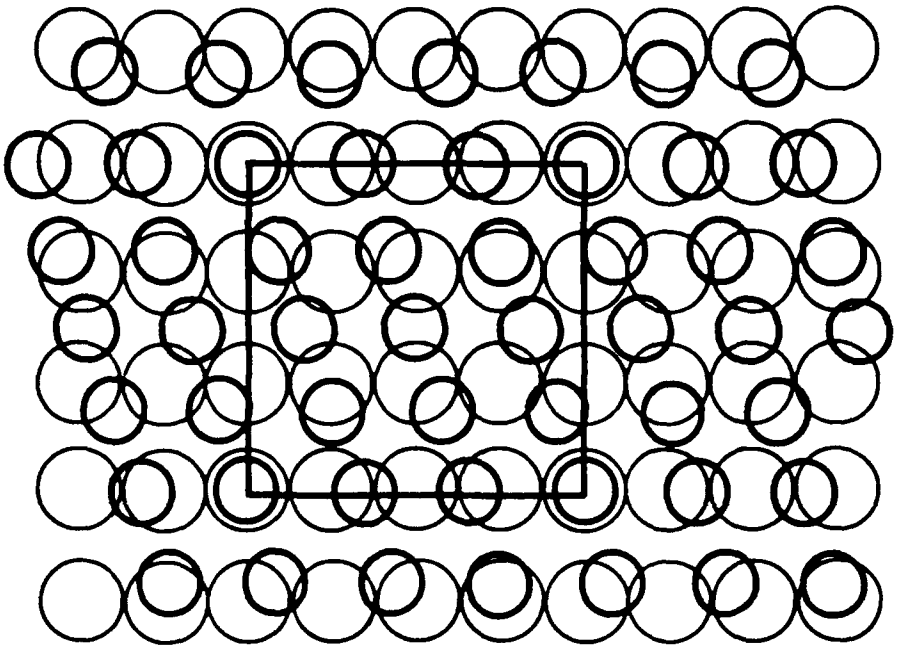

FIG 3

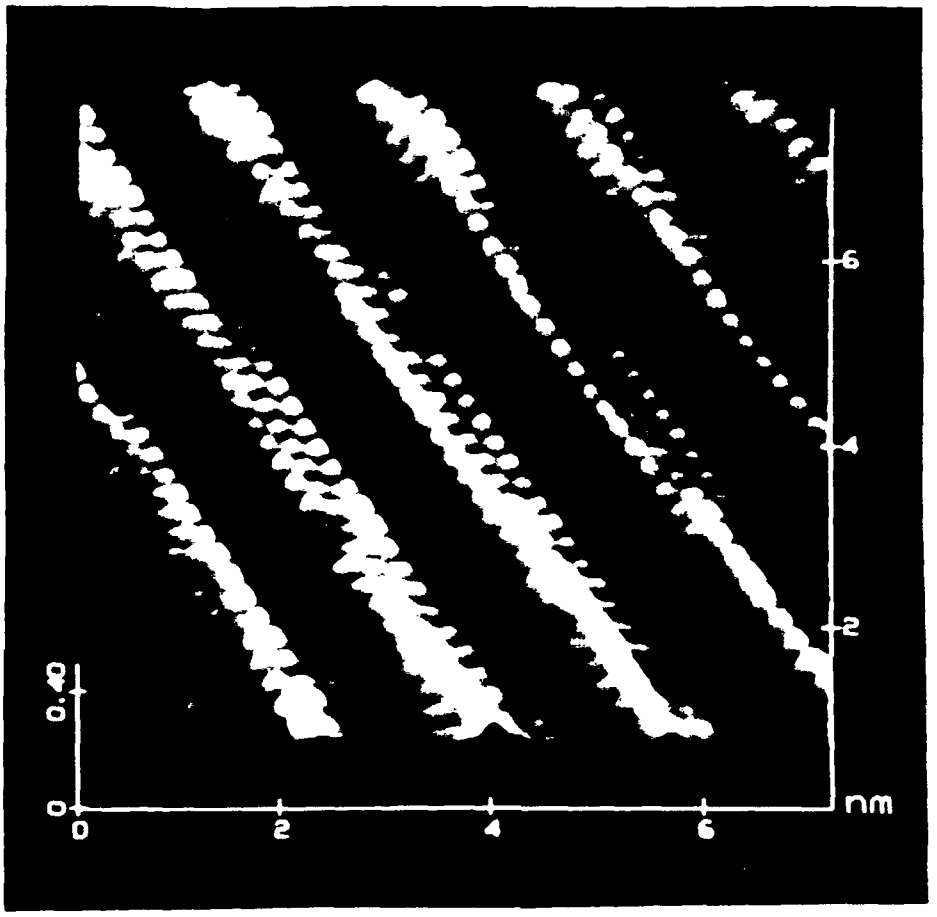

FIG 4

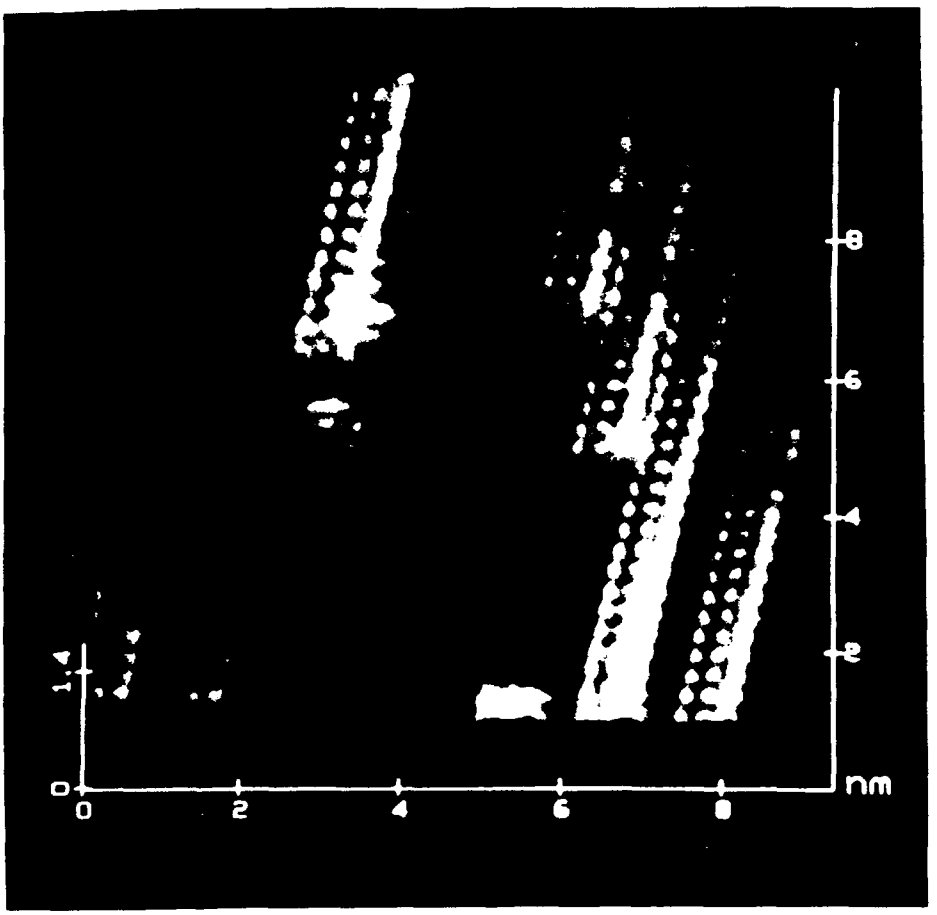

FIG 5